ARTICLES
PUBLISHED ONLINE: 22 DECEMBER 2013 | DOI: 10.1038/NMAT3828
nature materials

Spin-filtered edge states with an electrically tunable gap in a two-dimensional topological crystalline insulator

Junwei Liu[1,2], Timothy H. Hsieh[2], Peng Wei[2,3], Wenhui Duan[1], Jagadeesh Moodera[2,3] and Liang Fu[2]*

Three-dimensional topological crystalline insulators were recently predicted and observed in the SnTe class of IV–VI semiconductors, which host metallic surface states protected by crystal symmetries. In this work, we study thin films of these materials and expose their potential for device applications. We demonstrate that thin films of SnTe and $Pb_{1-x}Sn_xSe(Te)$ grown along the (001) direction are topologically non-trivial in a wide range of film thickness and carry conducting spin-filtered edge states that are protected by the (001) mirror symmetry through a topological invariant. Application of an electric field perpendicular to the film will break the mirror symmetry and generate a bandgap in these edge states. This functionality motivates us to propose a topological transistor device in which charge and spin transport are maximally entangled and simultaneously controlled by an electric field. The high on/off operation speed and coupling of spin and charge in such a device may lead to electronic and spintronic applications for topological crystalline insulators.

Crystal structure and symmetry play a fundamental role in determining the electronic properties of quantum materials. The interplay between crystallography and electronic topology[1,2] has advanced our understanding of topological insulators[3–5]. More recently, a new type of topological phases termed topological crystalline insulators[6] (TCIs) has been predicted[7] and observed[8–10] in three-dimensional (3D) materials SnTe and $Pb_{1-x}Sn_xSe(Te)$. A key characteristic of TCIs is the presence of metallic boundary states that are protected by crystal symmetry, rather than time reversal[11]. As a consequence, these states can acquire a bandgap under perturbations that break the crystal symmetry[7,12]. This property opens up the unprecedented functionality of tuning the charge and spin transport of topological boundary states with high on/off speed by applying an electric field. Here we theoretically demonstrate that thin films of SnTe and $Pb_{1-x}Sn_xSe(Te)$ grown along the (001) direction realize a new, 2D TCI phase that supports spin-filtered edge states with a bandgap tunable by the electric field effect. Our work may thus enable electronic and spintronic device applications based on TCIs.

TCIs have so far only been realized in 3D materials[7–10]. In this work, we propose a material realization of a 2D TCI phase, which is topologically distinct from an ordinary insulator in the presence of mirror symmetry about the 2D plane. The topology here is mathematically characterized by two integer topological invariants N_+ and N_-, which are Chern numbers of Bloch states with opposite mirror eigenvalues. Whereas the sum $N_+ + N_-$ determines the quantized Hall conductance, the mirror Chern number[2] defined by $N_M \equiv (N_+ - N_-)/2$ serves as an independent topological index[7,13–18], which distinguishes a mirror-symmetric TCI in two dimensions.

The mirror eigenvalue of an electron wavefunction is intimately related to its spin. As performing mirror transformation (denoted by M) twice is equivalent to a 2π rotation that changes the sign of a spinor, $M^2 = -1$ and hence mirror eigenvalues are either i or $-i$. In the absence of spin–orbit coupling, these two eigenvalues correspond to spin eigenstates $s_z = \pm 1/2$ where the quantization axis z is perpendicular to the plane, so that the mirror Chern number N_M reduces to the spin Chern number[19–21]. More broadly, the mirror Chern number can be defined for any system that is symmetric under reflection, with or without spin conservation. For instance, the quantum spin Hall state in graphene proposed in refs 22,23 is characterized by $|N_M| = 1$, in addition to the Z_2 index.

In this work, we demonstrate that (001) thin films of TCI SnTe and $Pb_{1-x}Sn_xSe(Te)$ in a wide range of thickness realize a 2D topological phase indexed by mirror Chern number $|N_M| = 2$, which supports two pairs of spin-filtered edge states. This new topological phase belongs to a different symmetry class from the quantum spin Hall state, and its edge states are protected solely by mirror symmetry instead of time reversal. A unique consequence is that applying an electric field perpendicular to the film breaks the mirror symmetry and generates a bandgap in these edge states. This functionality leads to a new way of controlling the charge and spin transport simultaneously by the electric field effect in a 2D TCI.

Our results are based on a combination of $k \cdot p$ modelling, band-structure calculations and topological band theory. A detailed derivation of the following analysis can be found in the Methods. Here, we describe how the competition between the inverted band structure in the 3D limit and hybridization between the two surfaces determines the topological nature of the TCI film as a function of film thickness. SnTe and $Pb_{1-x}Sn_xTe$ films are typically grown by molecular beam epitaxy in a layer-by-layer mode with good thickness control[24–26].

Three-dimensional TCIs, SnTe or $Pb_{1-x}Sn_xSe(Te)$, have Dirac fermion surface states on the (001) surface. There are four Dirac points located at non-time-reversal-invariant momenta Λ near the

[1]Department of Physics and State Key Laboratory of Low-Dimensional Quantum Physics, Tsinghua University, Beijing 100084, China, [2]Department of Physics, Massachusetts Institute of Technology, Cambridge, Massachusetts 02139, USA, [3]Francis Bitter Magnet Lab, Massachusetts Institute of Technology, Cambridge, Massachusetts 02139, USA. *e-mail: liangfu@mit.edu

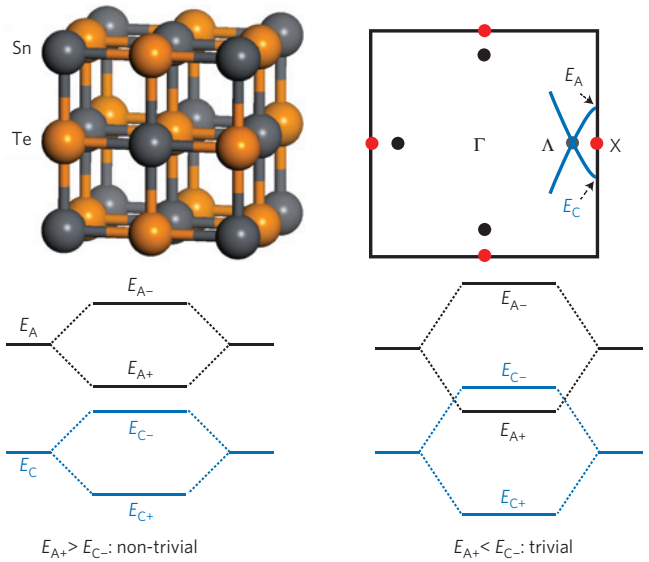

Figure 1 | Energy-level diagram of TCI thin films. Top: rocksalt structure of SnTe (left) and schematic Brillouin zone of the (001) surface of 3D SnTe (right). Four massless Dirac points of surface states are indicated by the black dots. Bottom: schematic of the conduction and valence bands of a TCI film at the X point. When the top and bottom surfaces hybridize weakly, the film inherits the inverted bandgap of the 3D limit (left). Strong hybridization drives a band crossing, leading to a trivial phase (right). A, C denote anion/cation, and ± denote bonding/anti-bonding combinations of the two surfaces.

X points, which can be derived from the $k \cdot p$ theory at the X point[27]. Surface states at X correspond to p orbitals of the cation (C) and the anion (A) respectively. Importantly, TCI has an inherently inverted band ordering opposite to the ionic insulator PbTe (ref. 7), so that the anion-derived surface state $E_A(X)$ is located near the conduction band edge, and the cation-derived surface state $E_C(X)$ near the valence band edge[30]. As we will show below, the topological properties of TCI (001) films are dictated by these gapped surface states at X, whereas their low-energy band structures are largely determined by the gapless states at Λ.

In this work, we consider TCI (001) films with an odd number of atomic layers, which are symmetric under the reflection $z \to -z$ about the 2D plane in the middle (Fig. 1). Our main result—gapless edge states with an electrically tunable gap—also holds for TCI films with an even number of layers, although the underlying symmetry is different and to be described elsewhere. When the film thickness is below the penetration length of surface states, the wavefunction hybridization between the top and bottom surfaces results in an energy splitting between the bonding and anti-bonding states. These hybridized surface states form the conduction and valence bands of the 2D TCI film. On the basis of $k \cdot p$ analysis (see Methods) and band-structure calculations, we find that the conduction and valence bands of the TCI film at the X point are derived from the bonding state of the anion at energy $E_{A+}(X)$ and the anti-bonding state of the cation at energy $E_{C-}(X)$. Owing to their opposite parity, the two bands $E_{A+}(X)$ and $E_{C-}(X)$ do not repel each other. The band ordering of $E_{A+}(X)$ and $E_{C-}(X)$ depends crucially on the competition between the hybridization of the two surfaces and the inverted gap $2m$ of each surface. For thick films, the hybridization is weak so that $E_{A+}(X) > E_{C-}(X)$. With this ordering, the band structure of the TCI film is adiabatically connected to the original surface states in the 3D limit, which is inherently inverted near X points (Fig. 1).

We now concentrate on the band inversion near the transition point $E_{A+}(X) \sim E_{C-}(X)$, which occurs at a critical film thickness to be determined from band-structure calculations later. This transition is described by Dirac mass reversal in a $k \cdot p$ Hamiltonian:

$$H(\mathbf{k}) = (\tilde{v}_x k_x s_x - \tilde{v}_y k_y s_y)\tau_x + \tilde{m}\tau_z \qquad (1)$$

where $\tau_z = \pm 1$ denotes the conduction and valence band of the TCI film at X, and each band has a Kramers degeneracy labelled by s_z. The velocities $\tilde{v}_x, \tilde{v}_y$ and the Dirac mass $\tilde{m} \equiv E_{C-}(X) - E_{A+}(X)$ are derived from microscopic parameters of surface states in the 3D TCIs and their hybridization strengths (see Methods for details).

Importantly, $H(\mathbf{k})$ is invariant under mirror symmetry about the 2D plane:

$$MH(\mathbf{k})M^{-1} = H(\mathbf{k})$$

Here the mirror operator is given by $M = -is_z\tau_z$, because bonding and anti-bonding states have opposite mirror eigenvalues, and so do spin-up and -down states. For a single-flavour Dirac fermion, sign reversal of Dirac mass $\tilde{m}$ changes the mirror Chern number N_M by 1 (ref. 2). We further take into account that there exist two X points in the Brillouin zone, related by a four-fold rotation. As a result of the simultaneous band inversions at both X points, N_M changes by 2:

$$|N_M(\tilde{m} > 0) - N_M(\tilde{m} < 0)| = 2$$

Combining this equation with the inverted band structure of $\tilde{m} < 0$ deduced earlier, we conclude that (001) thin films of TCIs with an inverted band ordering $E_{A+}(X) > E_{C-}(X)$ realize a 2D TCI phase with mirror Chern number $|N_M| = 2$.

The above conclusion drawn from $k \cdot p$ analysis and topological band theory is confirmed by our band-structure calculations of (001) TCI films based on a realistic tight-binding model[31], using SnTe as a representative. Figure 2 shows the band structures and orbital characters near the X point for 3- and 5-layer films, as well as a thick 25-layer film. Clearly, the 5-layer film has an inverted band ordering with the conduction (valence) band near X derived from the anion (cation), whereas the 3-layer film does not. This confirms our $k \cdot p$ result that the increased hybridization strength in thinner films drives the system out of the inverted regime. We further calculate the mirror Chern number numerically by integrating the Berry curvature over the Brillouin zone (see Methods), and confirm that $N_M = 0$ for the 3-layer film and $|N_M| = 2$ for the 5-layer film.

As the film thickness increases above 5 layers, the bandgap at X, $E_g(X) \equiv E_{A+}(X) - E_{C-}(X)$, increases monotonically, and eventually reaches the value 220 meV that is determined by the band structure of surface states in the 3D limit. Meanwhile, the fundamental bandgap in thicker films shifts from X to the momentum Λ located on the line ΓX, see, for example, the band structure of the 25-layer film shown in Fig. 2. In the 3D limit, the gap at Λ decreases to zero, thus recovering zero-energy Dirac points of TCI surface states (Fig. 3). Irrespective of this shift of bandgap, films thicker than 5 layers all show an inverted band structure near the X point, which results in the non-trivial band topology. This leads to a robust 2D TCI phase in a wide range of thickness. Moreover, the inverted gap in an 11-layer SnTe film reaches 0.15 eV near the X point, which is much larger than that of existing quantum spin Hall insulators. The same physics holds for $Pb_{1-x}Sn_xSe$ and $Pb_{1-x}Sn_xTe$, although the critical thickness depends on material details.

A hallmark of 2D TCIs is the presence of conducting edge states. The mirror Chern number $|N_M| = 2$ dictates that there exist two pairs of counter-propagating edge states within the bandgap, and those moving in the same (opposite) direction carry identical (opposite) mirror eigenvalues. This is confirmed in our band-structure calculation of a SnTe thin film in a strip geometry parallel to [100], using the recursive Green's function method[32]. As shown in Fig. 4, edge states with opposite mirror eigenvalues cross each

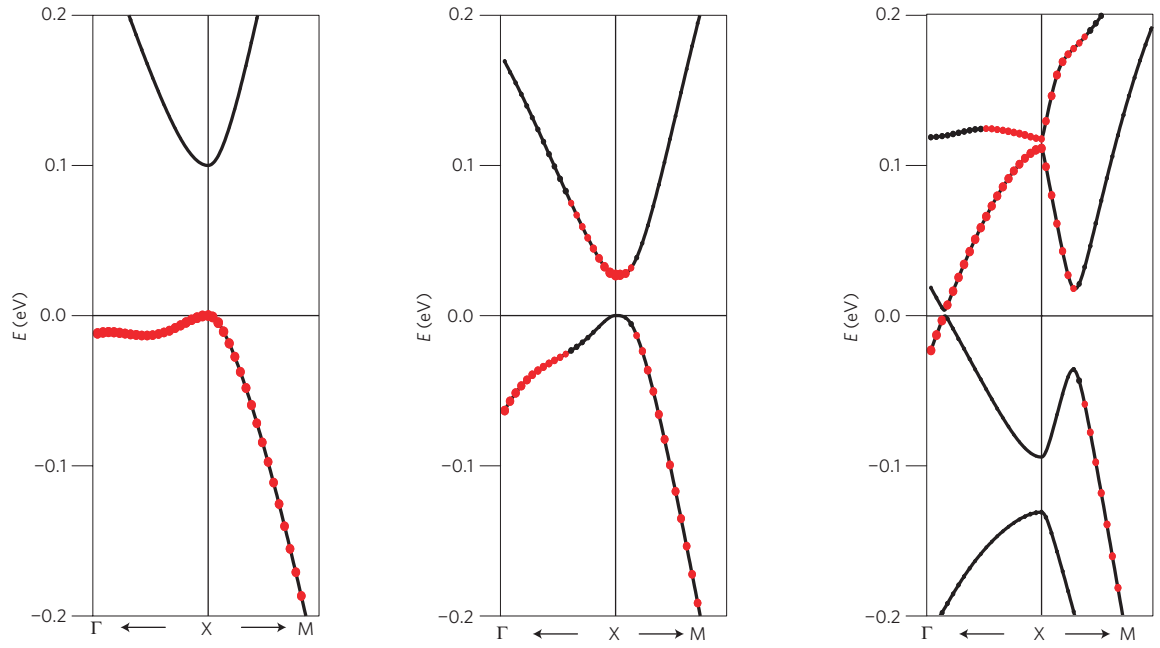

Figure 2 | Band inversion in SnTe films. Conduction and valence bands of a 3-layer (left), 5-layer (middle) and 25-layer (right) SnTe film. Red dots denote the weight of the electronic wavefunction on the anion Te. Starting from 5 layers, TCI (001) films show an inverted band structure relative to an ionic insulator.

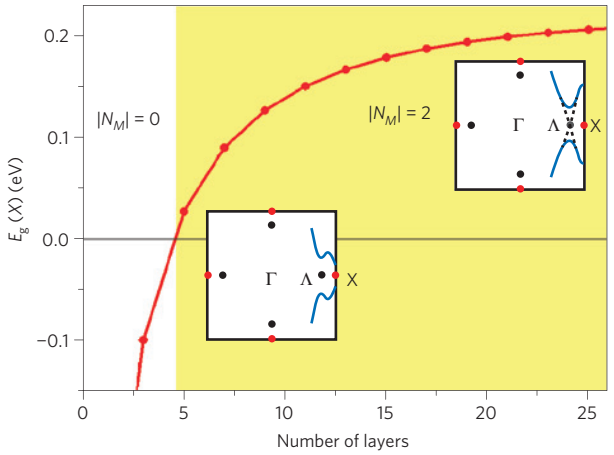

Figure 3 | Phase diagram of 2D TCIs. Bandgap of SnTe at the X point as a function of film thickness. Above five layers, the gap of SnTe at X is inverted and increases with thickness, resulting in a wide region of topologically non-trivial 2D TCI phase with mirror Chern number $|N_M| = 2$. For thick films, the fundamental bandgap shifts from X to Λ, where the Dirac points of 3D surface states are located (insets).

other at a pair of momenta in the edge Brillouin zone. In the ballistic limit, the conductance through such edge states is $2e^2/h$.

Unlike helical edge states in a quantum spin Hall insulator, the band crossings of spin-filtered edge states found here are located at non-time-reversal-invariant momenta, so that they are protected solely by the mirror symmetry $z \to -z$, but not time reversal. This leads to a remarkable consequence: applying a perpendicular electric field, which breaks the mirror symmetry, will generate a bandgap in these edge states. To illustrate this effect and estimate its magnitude, we calculate the band structure of an 11-layer SnTe film under a modest, uniform electric field that generates a 0.1 V potential difference across the film. The effect of an external electric field is modelled by adding a layer-dependent potential that varies linearly in the (001) direction to the tight-binding model[31]. We find that the spin-filtered edge states become completely gapped (Fig. 4). For comparison, a magnetic field or induced ferromagnetism is required to gap helical edge states of a quantum spin Hall insulator, which can be difficult to achieve[33].

Thus, edge-state transport in the 2D TCI phase found here has the unique property that the conductance is easily and widely tunable through an electric-field-induced gap instead of carrier depletion. This mechanism works at high on/off speed and improves power efficiency. As the on/off states originate from the crystal symmetry and symmetry breaking, they are more robust to material imperfections, which may also increase the operating cycles and improve the performance of the transistor especially at high frequency. In addition, only a local electric field is required to open up a gap for edge states, which further minimizes power consumption. The resistance of the off state depends on the amount of impurity states inside the energy gap, and thus the on/off ratio can be improved by controlling the film quality[34]. On the other hand, in the ballistic transport regime, the on/off ratio of the topological transistor can be further enhanced with a quantized on state conductance of $2e^2/h$ per edge and a negligible off state conduction.

As the electron spin polarization in the z direction is proportional to the mirror eigenvalue, an electric current carried by the TCI edge states is spin-polarized, and reversing the current flips the spin (Fig. 5). Importantly, it is the mirror eigenvalue, rather than the amount of spin polarization, that determines spin transport. For instance, when a TCI is placed adjacent to a ferromagnetic lead, $s_z = +1/2$ electrons in the lead will tunnel into the right-moving TCI edge states with mirror eigenvalue $+i$ with 100% certainty, if the set-up preserves the $z \to -z$ mirror symmetry.

The above functionality motivates us to propose a topological transistor device made of dual-gated TCI thin films, as shown in Fig. 5. The device on state in Fig. 5 itself can be used as a spin diode that enables the electric field control of the electron spin polarization. Using the two gates, one can control the electric field across the film and the carrier density independently, and thus turn on and off the coupled charge and spin transport by purely electrical means functioning as a transistor.

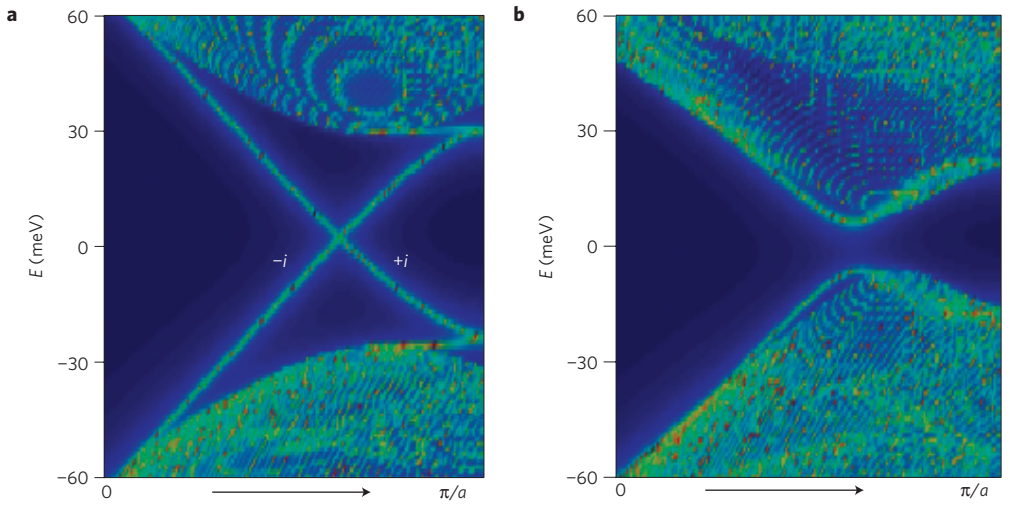

Figure 4 | Effect of electric field on edge states. Edge states of a TCI film and electric-field-induced gap. **a**, Bulk and gapless edge dispersion of an 11-layer SnTe film, labelled by mirror eigenvalues. **b**, Gapped dispersion when a perpendicular electric field is applied to generate a potential difference of 0.1 V across the film.

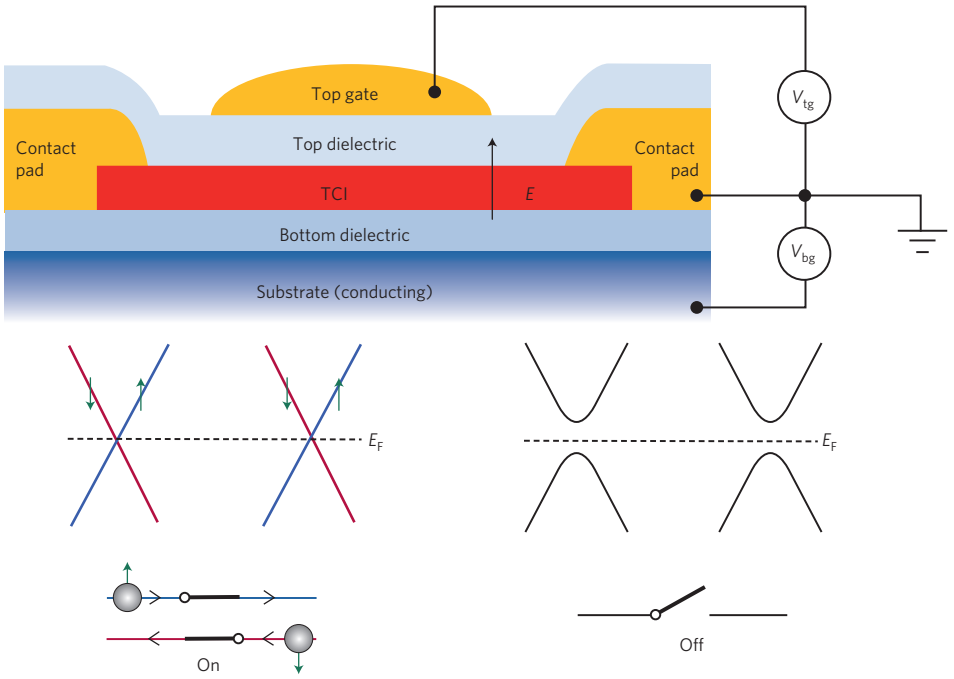

Figure 5 | Topological transistor. Proposed topological transistor device for using an electric field to tune charge and spin transport. Without an electric field, the TCI film has mirror symmetry and thus protected, spin-filtered edge states (left). Applying an electric field perpendicular to the film breaks the mirror symmetry, which generates a gap for the edge states (right). V_{tg}, top-gate voltage; V_{bg}, bottom-gate voltage; E_F, the Fermi level.

In addition to an electric field, a magnetic field can also be applied to a TCI thin film to independently control the dispersion of the two sets of edge modes. Consider the (100) edge states with crossings at $\pm k_0$, and apply a magnetic field $B=(B_\parallel, B_\perp, B_z)$ (parallel being along the edge). B_z will shift both the energies and momenta of these crossings, whereas in-plane magnetic field $B_\parallel$ and $B_\perp$ open up gaps. By tuning both electric and magnetic fields, the gaps at $\pm k_0$ can be separately tuned in the full range:

$$\Delta_{k_0} = \sqrt{(m_E + m_{B_\perp})^2 + m_{B_\parallel}^2} \quad (2)$$

$$\Delta_{-k_0} = \sqrt{(-m_E + m_{B_\perp})^2 + m_{B_\parallel}^2} \quad (3)$$

Here $m_E, m_{B_\perp}$ and $m_{B_\parallel}$ are energy gaps that are generated separately from the corresponding fields (see Methods).

From the material standpoint, thin films of IV–VI semiconductors have been grown epitaxially[24–26] and extensively studied[35]. In particular, ultrathin SnTe quantum wells have been made with high quality[36–38]. Related materials PbTe, PbSe and PbS, while topologically trivial in bulk form, can become inverted in strained thin films[7], which further broadens the material base available for use. Quantum devices based on IV–VI semiconductor quantum wells have been fabricated, which show ballistic transport with remarkable conductance quantization[39]. These developments as well as the ongoing interest in TCI thin films[40,41] give us hope that the 2D TCI phase and topological transistor device proposed here can be experimentally realized in the future.

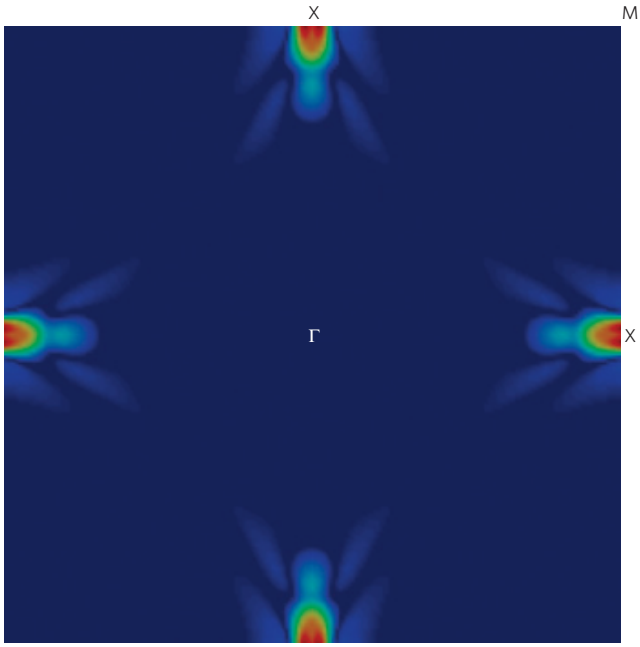

Figure 6 | Berry curvature. Plot of Berry curvature associated with $+i$ mirror eigenstates of a five-layer SnTe film over the 2D Brillouin zone. The $-i$ mirror eigenstates have opposite Berry curvatures. This makes the total Chern number zero, but the mirror Chern number $|N_M| = 2$.

Methods

In this section, we present a detailed derivation of $k \cdot p$ theory for TCI film; computation of the mirror Chern number; and effective theory for TCI edge states under electric and magnetic fields.

Derivation of $k \cdot p$ theory for TCI film. Here we provide the derivation leading up to the effective Hamiltonian (equation (1)). The starting point is (001) topological surface states of TCIs in the 3D limit. The $k \cdot p$ Hamiltonian for these surface states, linearized at an X point, is given by:

$$H_0(\mathbf{k}) = (v_x k_x s_y + v'_x k_x s_z \tau_x - v_y k_y s_x)\sigma_z + m\tau_z \tag{4}$$

$\sigma_z = \pm 1$ denote the top/bottom (001) surfaces, $\tau_z = 1(-1)$ denote basis states that are mainly derived from the cation(anion), and $s_z = \pm 1$ denotes a Kramers doublet. For a given value of σ_z, $H_0(\mathbf{k})$ reduces to the four-band $k \cdot p$ Hamiltonian for a single surface, derived in refs 27–29. Note, however, for technical convenience, we have chosen a basis different from that in ref. 27, such that $H_0(\mathbf{k}=0)$ is diagonal.

$H_0(\mathbf{k})$ is invariant under the symmetry operations of inversion P, $M_z : z \to -z$, $M_x : x \to -x$, $M_y : y \to -y$, two-fold rotation about z-axis C_2, and time-reversal Θ. In the above basis, these are represented by

$$P = \sigma_x, \quad M_z = -is_z\tau_z\sigma_x, \quad M_x = -is_x$$
$$M_y = -is_y\tau_z, \quad C_2 = -is_z\tau_z, \quad \Theta = is_y K$$

Hybridization between the two surfaces corresponds to off-diagonal terms in the σ_z basis. There are three hybridization terms allowed by the above symmetries:

$$H_h(\mathbf{k}) = \delta_1\sigma_x + \delta'_1\tau_z\sigma_x + \delta_2 s_x\tau_y\sigma_x \tag{5}$$

Here $\delta_1 \pm \delta'_1$ is the intra-orbital hybridization matrix element within the cation (anion) orbitals on the top and bottom surface. δ_2 is the inter-orbital hybridization matrix element between the cation and anion orbitals on the two surfaces. By combining (4) and (5), we obtain an eight-band $k \cdot p$ Hamiltonian for the (001) thin film of TCIs:

$$H_t(\mathbf{k}) = H_0(\mathbf{k}) + H_h(\mathbf{k})$$

The intra-orbital hybridization δ_1 and δ'_1 splits a pair of degenerate states at X on the two surfaces, $E_{\alpha=C,A}(X)$, into bonding and anti-bonding states with energies $E_{\alpha+}(X)$ and $E_{\alpha-}(X)$, respectively. From band-structure calculations, we find that δ'_1 is smaller than δ_1, so that the bonding states have a lower energy than the anti-bonding states: $E_{\alpha+}(X) < E_{\alpha-}(X)$. In this case, the conduction and valence band edges at X are derived from the bonding combination of the anions at energy $E_{A+}(X)$ and the anti-bonding orbital of the cations at energy $E_{C-}(X)$.

The transition as these two levels cross each other can be derived by projecting $H_t(\mathbf{k})$ into the low-energy subspace of $E_{A+}(X)$ and $E_{C-}(X)$. We find that δ'_1 plays an insignificant role and can be set to zero for simplicity. Projecting onto the four bands yields the $k \cdot p$ Hamiltonian for TCI film, equation (1)

$$H(k) = \tilde{m}\tau_z + (\tilde{v}_x k_x s_x - \tilde{v}_y k_y s_y)\tau_x$$

where the parameters are given by

$$\tilde{m} = \sqrt{m^2 + \delta_2^2} - |\delta_1|, \quad \tilde{v}_x = v'_x \mathrm{sgn}(\delta_1\delta_2), \quad \tilde{v}_y = \frac{v_y|\delta_2|}{\sqrt{m^2+\delta_2^2}}$$

Mirror Chern number. The mirror Chern number n_M is determined by the difference in Chern numbers N_+ and N_- that are associated with different mirror eigenstates. We compute these Chern numbers by numerically integrating the Berry curvature for all occupied bands over the entire 2D Brillouin zone[42]. The Bloch wavefunctions are obtained from the tight-binding model for SnTe (ref. 31). We find that the Berry curvature is strongly concentrated in the vicinity of two X points (Fig. 6), which justifies our analysis of band topology based on $k \cdot p$ theory.

We now comment on the sign of the mirror Chern number. To define the sign of N_M requires first choosing an orientation for the mirror plane. This is because: mirror operation is defined as spatial inversion combined with a two-fold rotation with respect to an axis normal to the mirror plane; and for a spin-1/2 particle, the eigenvalue of two-fold rotation $\pm i$ changes sign when the axis is reversed. Therefore, the absolute value of the mirror Chern number *per se* is meaningful only after specifying the orientation of the mirror plane, and N_M changes sign when one changes the choice of orientation. Nonetheless, the relative sign of the mirror Chern number and the electron's spin component along the mirror axis is unambiguous and measurable: it determines the directionality of spin current at the edge. We leave a detailed study of the sign of the mirror Chern number in TCI films to future work.

$k \cdot p$ theory for edge states. We now derive the $k \cdot p$ theory of the gapless edge states, to analyse how they are affected by external fields. Note that above, the x direction is actually (110) with respect to crystal axes. Let us now choose x to be (100) and analyse the gapless edge states with crossings at $\pm k_0$ along this axis.

The two symmetries that fix a single valley are M_z and $M_x\Theta$, and we choose the representation

$$M_z = -is_z$$
$$M_x\Theta = is_z K$$

The following table denotes how the electric field E (in the z direction) and magnetic field (B_x, B_y, B_z) transform under the two symmetries:

	M_z	$M_x\Theta$
E	−	+
B_x	−	−
B_y	−	+
B_z	+	+

The most general $k \cdot p$ Hamiltonian compatible with the above is

$$H_{k_0}(k) = vks_z + m_E s_y + m_{B_\parallel} s_x + m_{B_\perp} s_y + E_{B_z} + E'_{B_z} s_z \tag{6}$$

where v is the velocity of the edge states, and $m_E, m_{B_\parallel}, m_{B_\perp}, E_{B_z}$ and E'_{B_z} are linearly proportional to the corresponding electric/magnetic field. Using time-reversal symmetry, we obtain the $k \cdot p$ Hamiltonian for the other valley at $-k_0$:

$$H_{-k_0}(k) = vks_z - m_E s_y + m_{B_\parallel} s_x + m_{B_\perp} s_y - E_{B_z} + E'_{B_z} s_z \tag{7}$$

By diagonalizing equations (6) and (7), we derive the field-induced gap defined by equations (2) and (3) at the two valleys.

Received 10 September 2013; accepted 31 October 2013; published online 22 December 2013

References

1. Fu, L. & Kane, C. L. Topological insulators with inversion symmetry. *Phys. Rev. B* **76,** 045302 (2007).
2. Teo, J. Y. C., Fu, L. & Kane, C. L. Surface states and topological invariants in three-dimensional topological insulators: Application to $Bi_{1-x}Sb_x$. *Phys. Rev. B* **78,** 045426 (2008).
3. Hasan, M. Z. & Kane, C. L. Colloquium: Topological insulators. *Rev. Mod. Phys.* **82,** 3045–3067 (2010).

4. Qi, X. L. & Zhang, S. C. Topological insulators and superconductors. *Rev. Mod. Phys.* **83,** 1057–1110 (2011).
5. Moore, J. E. The birth of topological insulators. *Nature* **464,** 194–198 (2010).
6. Fu, L. Topological crystalline insulators. *Phys. Rev. Lett.* **106,** 106802 (2011).
7. Hsieh, T. H. *et al.* Topological crystalline insulators in the SnTe material class. *Nature Commun.* **3,** 982 (2012).
8. Tanaka, Y. *et al.* Experimental realization of a topological crystalline insulator in SnTe. *Nature Phys.* **8,** 800–803 (2012).
9. Dziawa, P. *et al.* Topological crystalline insulator states in $Pb_{1-x}Sn_xSe$. *Nature Mater.* **11,** 1023–1027 (2012).
10. Xu, S. Y. *et al.* Observation of a topological crystalline insulator phase and topological phase transition in $Pb_{1-x}Sn_xTe$. *Nature Commun.* **3,** 1192 (2012).
11. Mong, R. S. K., Essin, A. M. & Moore, J. E. Antiferromagnetic topological insulators. *Phys. Rev. B* **81,** 245209 (2010).
12. Okada, Y. *et al.* Observation of Dirac node formation and mass acquisition in a topological crystalline insulator. *Science* **341,** 1496–1499 (2013).
13. Takahashi, R. & Murakami, S. Gapless interface states between topological insulators with opposite dirac velocities. *Phys. Rev. Lett.* **107,** 166805 (2011).
14. Kargarian, M. & Fiete, G. A. Topological crystalline insulators in transition metal oxides. *Phys. Rev. Lett.* **110,** 156403 (2013).
15. Chiu, C-K., Yao, H. & Ryu, S. Classification of topological insulators and superconductors in the presence of reflection symmetry. *Phys. Rev. B* **88,** 075142 (2013).
16. Morimoto, T. & Furusaki, A. Topological classification with additional symmetries from Clifford algebras. *Phys. Rev. B* **88,** 125129 (2013).
17. Ye, M., Allen, J. W. & Sun, K. Topological crystalline Kondo insulators and universal topological surface states of SmB_6. Preprint at http://arxiv.org/abs/1307.7191 (2013).
18. Weng, H., Zhao, J., Wang, Z., Fang, Z. & Dai, X. Topological crystalline Kondo insulator in mixed valence ytterbium borides. Preprint at http://arxiv.org/abs/1308.5607 (2013).
19. Abanin, D. A., Lee, P. A. & Levitov, L. S. Spin-filtered edge states and quantum Hall effect in graphene. *Phys. Rev. Lett.* **96,** 176803 (2006).
20. Young, A. F. *et al.* Tunable symmetry breaking and helical edge transport in a graphene quantum spin Hall state. Preprint at http://arxiv.org/abs/1307.5104 (2013).
21. Maher, P. *et al.* Evidence for a spin phase transition at charge neutrality in bilayer graphene. *Nature Phys.* **9,** 154–158 (2013).
22. Kane, C. L. & Mele, E. J. Quantum spin Hall effect in graphene. *Phys. Rev. Lett.* **95,** 226801 (2005).
23. Kane, C. L. & Mele, E. J. Z_2 topological order and the quantum spin Hall effect. *Phys. Rev. Lett.* **95,** 146802 (2005).
24. Bauer, G. & Springholz, G. Molecular beam epitaxy of IV–VI semiconductor hetero- and nano-structures. *Phys. Status Solidi B* **244,** 2752–2767 (2007).
25. Abramof, E., Ferreira, S. O., Rappl, P. H. O., Closs, H. & Bandeira, I. N. Electrical properties of $Pb_{1-x}Sn_xTe$ layers with $0 \leqslant x > \leqslant 1$ grown by molecular beam epitaxy. *J. Appl. Phys.* **82,** 2405–2410 (1997).
26. Ishida, A. *et al.* Electrical and thermoelectrical properties of SnTe-based films and superlattices. *Appl. Phys. Lett.* **95,** 122106 (2009).
27. Liu, J., Duan, W. & Fu, L. Two types of surface states in topological crystalline insulators. *Phys. Rev. B* (in the press); preprint at http://arxiv.org/abs/1304.0430 (2013).
28. Fang, C., Gilbert, M. J., Xu, S-Y., Bernevig, B. A. & Hasan, M. Z. Theory of quasiparticle interference in mirror-symmetric two-dimensional systems and its application to surface states of topological crystalline insulators. *Phys. Rev. B* **88,** 125141 (2013).
29. Wang, Y. J. *et al.* Nontrivial spin texture of the coaxial Dirac cones on the surface of topological crystalline insulator SnTe. *Phys. Rev. B* **87,** 235317 (2013).
30. Safaei, S., Kacman, P. & Buczko, R. Topological crystalline insulator (Pb,Sn)Te: Surface states and their spin polarization. *Phys. Rev. B* **88,** 045305 (2013).
31. Lent, C. S. *et al.* Relativistic empirical tight-binding theory of the energy bands of GeTe, SnTe, PbTe, PbSe, PbS, and their alloys. *Superlatt. Microstruct.* **2,** 491–499 (1986).
32. Lopez Sancho, M. P., Lopez Sancho, J. M. & Rubio, J. Highly convergent schemes for the calculation of bulk and surface Green functions. *J. Phys. F* **15,** 851 (1985).
33. Du, L., Knez, I., Sullivan, G. & Du, R. Observation of quantum spin Hall states in InAs/GaSb bilayers under broken time-reversal symmetry. Preprint at http://arxiv.org/abs/1306.1925 (2013).
34. Lang, M. *et al.* Competing weak localization and weak antilocalization in ultrathin topological insulators. *Nano Lett.* **13,** 48–53 (2013).
35. Khokhlov, D. *Lead Chalcogenides: Physics and Applications* (CRC, 2002).
36. Ishida, A., Aoki, M. & Fujiyasu, H. Semimetallic Hall properties of PbTe–SnTe superlattice. *J. Appl. Phys.* **58,** 1901–1903 (1985).
37. Rogacheva, E. I. *et al.* Quantum size effects in *n*-PbTe/*p*-SnTe/*n*-PbTe heterostructures. *Appl. Phys. Lett.* **86,** 063103 (2005).
38. Taskin, A. A., Sasaki, S., Segawa, K. & Ando, Y. Topological surface transport in epitaxial SnTe thin films grown on Bi_2Te_3. Preprint at http://arxiv.org/abs/1305.2470 (2013).
39. Grabecki, G. *et al.* PbTe—A new medium for quantum ballistic devices. *Physica E* **34,** 560–563 (2006).
40. Fang, C., Gilbert, M. J. & Bernevig, B. A. Large Chern number quantum anomalous Hall effect in thin-film topological crystalline insulators. Preprint at http://arxiv.org/abs/1306.0888 (2013).
41. Zhang, F., Li, X., Feng, J., Kane, C. L. & Mele, E. J. Zeeman field-tuned transitions for surface chern insulators. Preprint at http://arxiv.org/abs/1309.7682 (2013).
42. Fang, Z. *et al.* The anomalous Hall effect and magnetic monopoles in momentum space. *Science* **302,** 92–95 (2003).

Acknowledgements

We thank Y. Ando and A. Young for helpful comments and suggestions. This work is supported by the US Department of Energy, Office of Basic Energy Sciences, Division of Materials Sciences and Engineering under Award DE-SC0010526. T.H.H. acknowledges support under NSF Graduate Research Fellowship No. 0645960. J.L and W.D. acknowledge support from the Ministry of Science and Technology of China (Grant Nos 2011CB921901 and 2011CB606405) and the National Natural Science Foundation of China (Grant No. 11074139). P.W. and J.M. are grateful for support from the MIT MRSEC through the MRSEC Program of the NSF under award number DMR-0819762, as well as NSF DMR grants 1207469 and ONR grant N00014-13-1-0301.

Author contributions

J.L. performed band-structure and mirror Chern number calculations. T.H.H. performed theoretical analysis with contributions from J.L. T.H.H. and L.F. wrote the manuscript with contributions from all authors. L.F. conceived and supervised the project. All correspondence should be addressed to L.F.

Additional information

Reprints and permissions information is available online at www.nature.com/reprints. Correspondence and requests for materials should be addressed to L.F.

Competing financial interests

The authors declare no competing financial interests.